Supplementary Material: Interfacial free energy as the key to the pressure-induced deceleration of ice nucleation

Jorge R. Espinosa[†], Alberto Zaragoza[†], Pablo Rosales-Pelaez[†], Caridad Navarro, Chantal Valeriani[†,‡], Carlos Vega[†] and Eduardo Sanz[†]
[†] *Departamento de Quimica Fisica I, Facultad de Ciencias Quimicas, Universidad Complutense de Madrid, 28040 Madrid, Spain.*
[‡] *Departamento de Fisica Aplicada I, Facultad de Ciencias Fisicas, Universidad Complutense de Madrid, 28040 Madrid, Spain.*

(Dated: August 27, 2016)

I. METHODS

A. Simulation details

We use the LAMMPS [1] and the GROMACS [2] Molecular Dynamics packages to simulate the mW [3] and TIP4P/Ice [4] models respectively. In GROMACS pressure is kept constant using an isotropic Parrinello-Rahman barostat[5] with a relaxation time of 0.5 ps. To fix the temperature we employ a velocity-rescale thermostat [6] with a relaxation time of 0.5 ps. The time step for the Verlet integration of the equations of motion is 3 fs. For the TIP4P/Ice model we use Particle Mesh Ewald Summations [7] to deal with electrostatic interactions. The cut-off radious for dispersive interactions and for the real part of electrostatic interactions is 9 Å. In LAMMPS temperature is kept constant with the Nose-Hoover thermostat [8] and pressure with the Nose-Hoover barostat [9], implemented as described in Ref. [10]. The relaxation time for both the thermostat and the barostat is 0.5 ps. The time step for the integration of the equations of motion is 5 fs.

B. Number of particles in the cluster

In order to compute the number of particles in the ice cluster we first identify particles with a solid-like environment and then find the largest cluster of such particles. To label particles as solid or liquid-like we use the local bond order parameters $\bar{q}_i$ proposed in Ref. [11] (i is the order of the spherical harmonics in $\bar{q}_i$). $\bar{q}_i$ is calculated with the coordinates of the tagged particle and those of its neighbors within a certain cut-off distance. A tagged particle is labelled as solid-like if its $\bar{q}_i$ is larger than a certain threshold, $\bar{q}_{i,t}$, and liquid-like otherwise. In order to chose $\bar{q}_{i,t}$ for a given thermodynamic state we compute the fraction of particles wrongly labelled in the bulk ice and liquid phase as a function of $\bar{q}_{i,t}$ and pick the value for which the fraction of mislabelled particles is the same in both phases. If such fraction is 0 for a certain range, we pick the middle value of the range. To distinguish liquid from ice Ih (ice 0) we use $i = 6$ ($i = 4$) and a cut-off distance of 3.5 Å (5 Å). The same cut-off distance has been considered to identify solid neighbors belonging to the same cluster. This procedure is explained in more detail in Refs. [12–15] for ice I. The value of the chosen $\bar{q}_{4,t}$ as a function of temperature to distinguish ice 0 from water for the mW model is shown in Fig. 1.

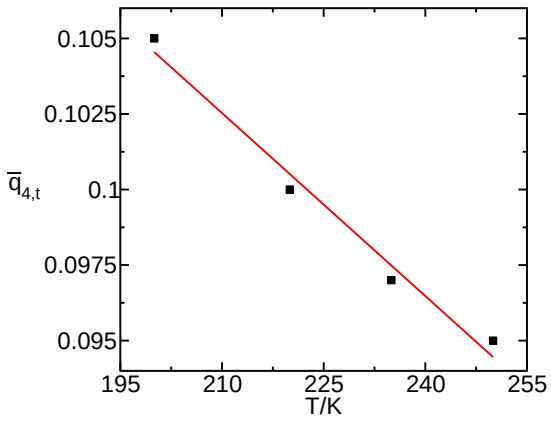

FIG. 1. $\bar{q}_{4,t}$ threshold as a function of temperature to distinguish ice 0 from water at 1 bar for the mW model.

II. ERROR ANALYSIS OF THE MAIN TEXT RESULTS

The main error source in our calculations of the nucleation rate is the uncertainty in the temperature at which the inserted clusters are found to be critical. We have run simulations for a 2.5 K temperature grid to enclose such temperature within a range of ± 1.25 K. In Fig. 2 we show in blue our seeding data ($\Delta T > 0$) for the interfacial free energy (triangles 1 bar and circles 2000 bar) and in magenta and green the corresponding values of γ if the clusters had found to be critical for a temperature 1.25 K higher and lower respectively. At $\Delta T = 0$ we plot in blue the value of γ obtained with the MI method [16, 17] and in green and magenta the upper and lower boundaries of the error bar for such calculation respec-

tively. To estimate an upper (lower) boundary for our linear fit to γ we take the green (magenta) points. The green fits, corresponding to high γ values, give rise to the lower boundary for J, indicated with a dashed line in Fig. 1(b) of the main text. On the other hand, the magenta $\gamma(T)$ fits give rise to the upper error boundary for J. The error bar for $J(\Delta T)$ is large for small ΔT because the slope of $J(\Delta T)$ is large for small supercooling. Dashed lines in Fig. 2 are linear fits that combine high values of γ at low ΔT with low values of γ at high ΔT or viceversa. The resulting fits are enclosed within the range defined by the fits to the green, i. e. high, and magenta, i. e. low, values of γ. Therefore, the most pessimistic estimate of the error bar for γ is given by the green and the magenta lines. Errors in γ have a strong effect in J since γ comes as a third power in $\Delta G_c/k_BT$ which, in turn, comes exponentially in J. Such functional dependency, along with the higher accuracy with which $|\Delta\mu(T)|$, $\rho_f(T)$, $\rho_s(T)$ and $f^+(T)$ are determined, causes that the impact of γ in the uncertainty of J is orders of magnitude higher that of the other variables affecting J.

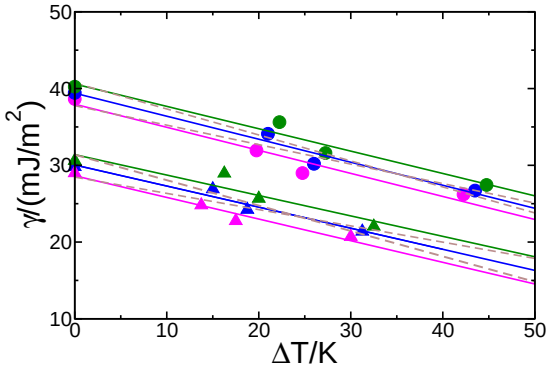

FIG. 2. Interfacial free energy as a function of ΔT for TIP4P/Ice at 1 bar (triangles) and 2000 bar (circles). Results for $\Delta T > 0$ ($\Delta T = 0$) have been obtained with seeding (MI). Blue symbols are the γ values corresponding to the ΔT at which the inserted clusters were found to be critical. Magenta (green) symbols are the γ values that would have been obtained if the clusters had been found to be critical at a ΔT 1.25 K lower (higher). Solid lines are linear fits to the symbols with the same color as the line. Dashed lines are linear fits that combine high values of γ at low ΔT with low values of γ at high ΔT or viceversa.

The statistical error described above should be complemented with a systematic error coming from the fact that the true number of particles in the cluster could be different from that detected by the employed order parameter. Our order parameter works well for particles in the middle of the cluster and particles in the bulk liquid. However, interfacial particles can be ascribed to one phase or the other depending on subtle changes in the order parameter threshold. Since the number of particles in the surface goes as $N^{2/3}$, we use $N^{2/3}$ as an estimate for the error in the number of particles in the critical cluster. Taking this error source into account the uncertainty boundaries for $\gamma(T)$ broaden as shown in Fig. 3(a) with the dotted curves, that consider both systematic and statistical errors. The relative error in the number of particles in the cluster, $N^{-1/3}$, goes to zero as the number of particles in the cluster goes to infinity. Therefore, the systematic error will affect small clusters to a greater extent than large ones. This explains why the distance between dotted and the dashed lines is negligible at $\Delta T = 0$ and increases with ΔT. Using the $\gamma(T)$ dependence given by the dotted lines in Fig. 3(a) we obtain the combined systematic-statistical error boundaries for J, indicated by the dotted lines in Fig. 3(b). Not even taking the systematic error into account we are able to conceal our estimate of J with the calculation reported in Ref. [18]. The fact that for a given supercooling the nucleation rate decreases with pressure is captured for any ΔT outside the systematic+statistical error bars. However, in the main text we deliberately do not include the systematic contribution to the error bar because our aim is to compare the nucleation rate for different pressures. A systematic error would affect both studied pressures in the same direction and including it would be deceptive when analysing the trend of J with pressure.

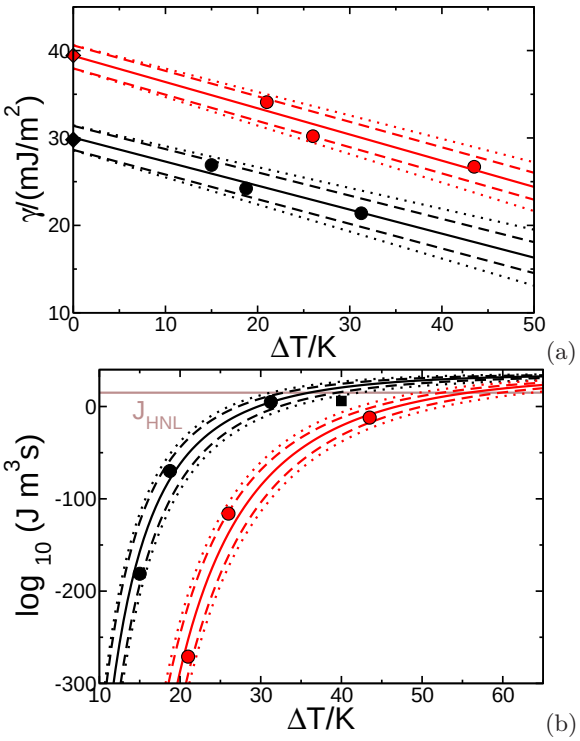

FIG. 3. Same as Figs. 1 (d) and (b) in main text but with added dotted lines that include in the error bar possible systematic deviations from the true number of particles in the critical cluster.

III. NUCLEATION VIA ICE IH WITH MW

Here we show that the explanation we find for the slowing down of ice nucleation with pressure for the TIP4P/Ice model (an increase of γ with pressure) also holds for mW water. Moreover, we compare the performance of both models in predicting the behaviour of real water. In Table I we give details on our seeding calculations with mW using spherical ice Ih clusters.

In Fig. 4(a) we show the ice nucleation rate as a function of the supercooling for different pressures. These curves were obtained by seeding the supercooled fluid with an ice Ih spherical cluster. The prediction of mW is that for a given supercooling the nucleation rate decreases with pressure. Therefore, the model is in qualitative agreement with the experimental trend and with the predictions by the TIP4P/Ice model. In Fig. 4(b) we show a zoom of Fig. 4(a) in the region of high supercooling, where we can compare the seeding predictions to the nucleation rate computed by means of brute force (BF) simulations of spontaneous ice nucleation (from Ref. [19] at 1 bar and from this work at 2000 and 5000 bar). We obtain a satisfactory agreement between seeding and BF for all pressures, which strongly supports the validity of the approach followed in this work.

In Fig. 5(a) we show the same as in Fig. 2 of the main text but including the mW data. Although mW qualitatively captures the experimental trend, the predictions made by the TIP4P/Ice model are in much better quantitative agreement with the experiment.

It is important to notice that the location of the HNL depends on the experimental set up. Specifically, it depends on the employed cooling rate, v, and on the volume of the system, V. Upon cooling, the time τ the sample spends at given temperature interval ΔT is the inverse of the cooling rate, v, times ΔT:

$$\tau = \frac{\Delta T}{v} \tag{1}$$

And, assuming that ΔT is small enough so that J is constant in the temperature interval, the time it takes for a critical nucleus to appear in the system in such temperature interval is:

$$\tau_N(T) = \frac{1}{VJ(T)}, \tag{2}$$

where T is the center of the temperature interval. The system will keep cooling down until $\tau_N(T)$ becomes smaller than τ. Thus, by equating both times and for $\Delta T = 1$K one gets the nucleation rate associated to the HNL is given by:

$$J(T_{HNL}) = \frac{v}{V} \tag{3}$$

As discussed in the main text, the experimental HNL defined in Ref. [21] is given by the points at which $\log_{10}(J\mathrm{m}^3\mathrm{s})$=15 (the rate associated to a cooling rate of 3K/min and microdroplets). The HNL defined in Ref. [22] is associated to a different nucleation rate given by: $J(T_{HNL}) = 1/(\tau_s V_s)$, where τ_s is the simulation time required to observe crystallization in a simulation box of volume V_s. Unfortunately, $J(T_{HNL})$ was not reported in Ref. [22], but typical values for $\log_{10}[J(T_{HNL})\mathrm{m}^3\mathrm{s}]$ in simulations are 32-33 (for simulations of a few nanoseconds for thousands of particles). In Fig. 5(b) we compare the simulation HNL defined in Ref. [22], HNLS, with the mW prediction of the experimental HNL, alongside the mW melting lines of ices 0 and I. The HNLS looks indeed parallel to the ice 0 melting line. However, the slope of the HNL depends on the nucleation rate with which it is associated. In fact, the mW prediction for the experimental HNL looks almost parallel to the ice I melting line rather than to the ice 0 one (although, as previously mentioned, the qualitative effect of the HNL having a larger negative slope than the ice Ih melting line is cap-

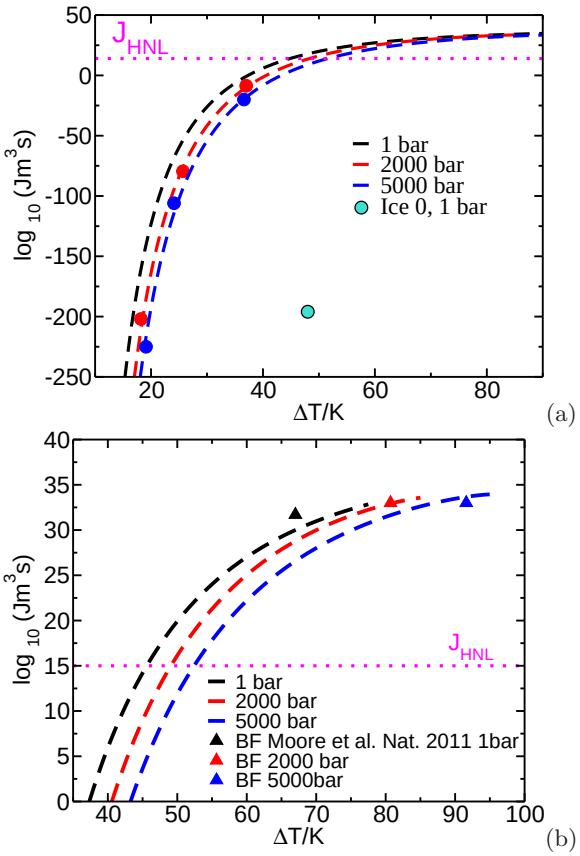

FIG. 4. Decimal logarithm of the ice nucleation rate as a function of the supercooling for different pressures. Symbols are calculations from seeding simulations and curves are CNT fits done as described in Refs. [13–15, 20]. The fit for 1 bar is taken from Ref. [13]. Fig. (b) is a zoom of Fig. (a) in the deep supercooling region where the seeding fits can be compared to brute force simulations (triangles). The horizontal dotted lines indicates the J associated to the HNL. All data correspond to ice Ih, except the cyan symbol that corresponds to ice 0 (note that ΔT refers to the ice Ih melting point).

p/bar	T/K	ΔT/K	N_c	$\Delta\mu$/(kcal/mol)	f^+/s^{-1}	$\rho_f/(g/cm^3)$	$\rho_s/(g/cm^3)$	$\gamma/(mJ/m^2)$	$\Delta G_c/(k_BT)$	$\log_{10}(Jm^3s)$
2000	233.8	36.9	660	0.1630	1.0×10^{14}	1.040	1.007	31.8	116	-8
2000	245.0	25.7	2334	0.1150	3.1×10^{14}	1.039	1.006	34.3	276	-80
2000	252.5	18.2	6794	0.0822	6.1×10^{14}	1.039	1.005	35.0	556	-202
5000	225.0	36.6	790	0.1560	4.0×10^{13}	1.081	1.043	33.2	138	-20
5000	237.5	24.1	3034	0.1043	1.2×10^{14}	1.078	1.042	34.8	335	-106
5000	242.5	19.1	7042	0.0839	6.0×10^{14}	1.077	1.041	37.0	613	-226

TABLE I. Variables involved in the calculation of the ice Ih nucleation rate and the water-ice Ih interfacial free energy of mW water. See main text for the meaning of all variables.

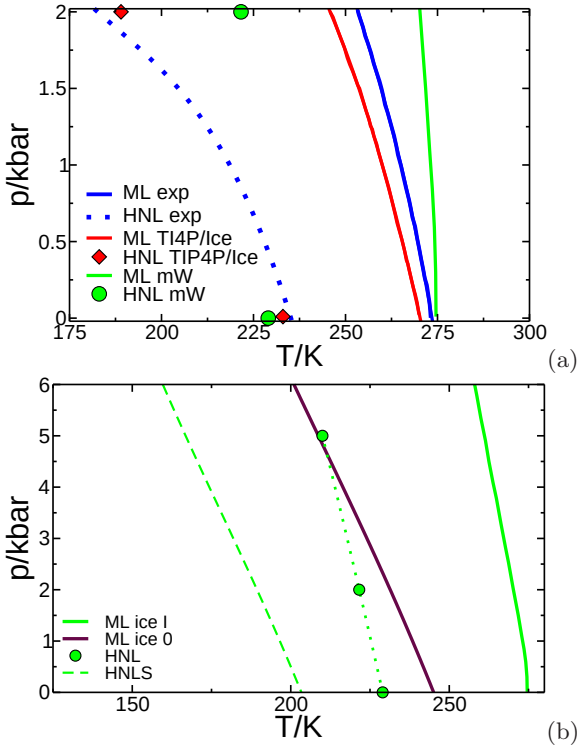

FIG. 5. (a) Same as Fig. 2 in the main text but with the results for the mW model in green. (b) Results for the mW alone including the ice 0 melting line and the simulation HNL from Ref. [22], HNLS.

tured by the mW model). Therefore, no firm conclusions can be drawn from a HNL being parallel to a melting line and it is just a coincidence that the HNLS is parallel to the ice 0 melting line.

In seeking the main reason for the decrease of the nucleation rate with pressure at constant supercooling we also find for the mW model that the ice-water interfacial free energy is the main factor. In Fig. 6(a) we show that the kinetic prefactor is not responsible for the decrease of the nucleation rate and that the reason must be found in $\exp(\Delta G_c/(k_BT))$. Fig. 6(a) also shows that the slowing down of the nucleation rate for TIP4P/Ice is much more pronounced than for mW. In Fig. 6(b), we analyse the importance of the different factors contributing to the ratio between $\exp(\Delta G_c/(k_BT))$ at 2000 and 1 bar. Such ratio (black curve) is lower for mW than for TIP4P/Ice The temperature factor (red curve) is smaller for mW because the melting line of mW has a smaller negative slope. The density factor (green curve) accelerates nucleation more than it does for in TIP4P/Ice because ice is more compressible for mW. As in the TIP4P/Ice case, the interfacial free energy (purple curve) justifies most of the increase of the nucleation barrier with pressure.

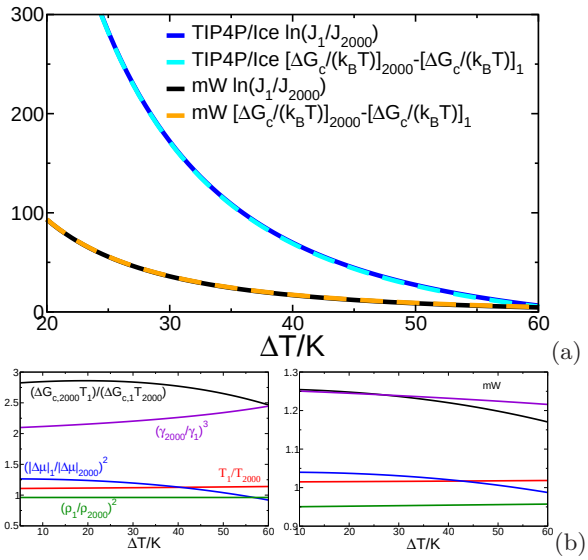

FIG. 6. Same as Fig. 3 in the main text but for the mW model. We include also the TIP4P/Ice results from the main text to facilitate the comparison. Notice the different scale for the TIP4P/Ice and the mW figures.

We show in Fig. 7(a) that γ indeed increases with pressure. Comparing this figure with Fig. 1(d) of the main text one can see that the predicted increase is lower for mW than for TIP4P/Ice. This is the main reason for the better quantitative performance of the TIP4P/Ice model shown in Fig. 5. We have double checked our estimation of γ by computing directly the interfacial free energy at coexistence with the MI method [16] (diamonds in Fig. 7(a)). For 1 bar we report the MI average value between the main crystal orientations (basal, primary prismatic and secondary prismatic) [17], whereas for 2000 and 5000 bar we report only the value for the basal plane. As for

TIP4P/Ice, we find a good agreement between seeding and MI, confirming the validity of our approach.

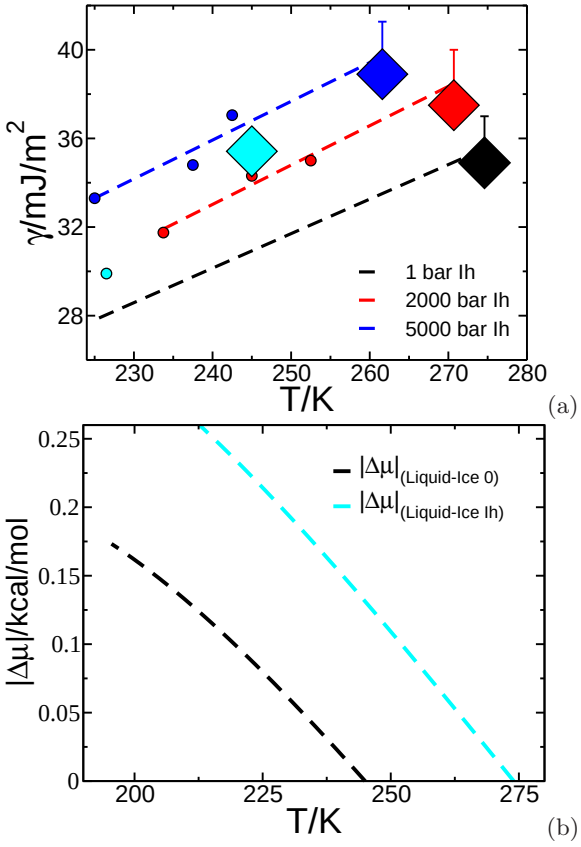

FIG. 7. (a) Water-ice Ih interfacial free energy as a function of temperature for the mW model at different pressures. Circles are seeding data and straight lines linear fits. Diamonds are direct calculations of γ at coexistence with the MI method [16] (errors are the size of the symbol). Results for ice Ih at 1 bar are taken from Ref. [15, 17]. All data correspond to ice Ih, except the cyan symbols that corresponds to ice 0 at 1 bar (circle and diamond from seeding and MI methods respectively). (b) Chemical potential difference between liquid and ices 0 and Ih as a function of temperature.

IV. NUCLEATION VIA ICE 0 WITH MW

In order to estimate the interfacial free energy for ice 0 we apply the seeding method to a spherical seed having ice 0 structure at 1 bar using the mW model. To illustrate how we find the temperature that makes the inserted cluster critical we show in Fig. 8 the number of particles in the cluster versus time for several temperatures. For temperatures higher than that at which the inserted cluster is critical, the cluster melts, whereas it grows for lower ones. Then, according to the results shown in Fig. 8, the inserted cluster is critical at T=226.5±2.5K. This is a supercooling of 18.5 K with respect to the ice 0 melting point of 245 K[22]. This result, alongside all variables needed for the calculation of the interfacial free energy, is reported in Table II. The obtained interfacial free energy is plotted in Fig. 7 (a). By comparing the obtained value to the fit of the water-ice Ih interfacial free energy at 1 bar it becomes evident that ice 0 has a higher interfacial free energy. This result, together with the fact that the chemical potential difference between the liquid and ice 0 is smaller that that between the liquid and ice Ih (Fig. 7(b)), rules out any possible involvement of ice 0 in ice nucleation. Moreover, by measuring directly the interfacial free energy using the MI method at coexistence for a planar interface (1 bar and 245K) we obtain 35.4 mJ/m^2, which confirms the higher value of γ for ice 0 compared to ice Ih (see cyan diamond in figure 7 (a)).

From our seeding study we can also estimate the rate for the nucleation pathway going through a critical cluster with ice 0 structure. This is plotted in Fig. 4 with a cyan circle, to be compared with the black solid line corresponding to the nucleation rate at 1 bar for Ih spherical critical clusters. Because both $\Delta\mu$ and γ are less favourable for the nucleation of ice 0 than of ice I, the formation of an ice 0 critical cluster is about 200 orders of magnitude slower than that of an ice Ih one.

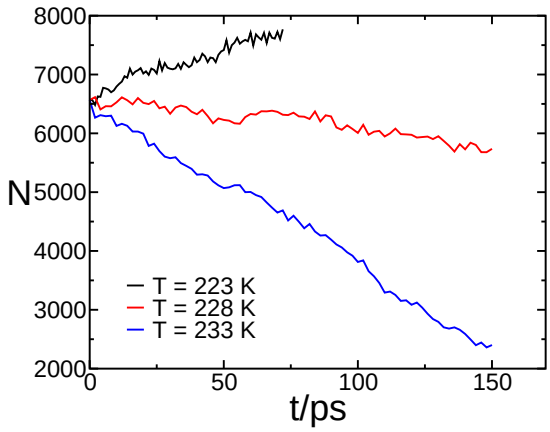

FIG. 8. Number of particles in the ice 0 cluster versus time for several temperatures at 1 bar (as indicated in the legend).

V. SURFACE STRUCTURE OF MW ICE IH CLUSTERS

In Ref. [22] critical clusters are found to have an ice I core surrounded by an ice 0 shell. This observation is not consistent with our result that the interfacial free energy of ice 0 with water is higher than that of ice I. We now look for ice 0 in the surface of our mW ice Ih seeds. Even though we initially insert an ice Ih seed, an ice 0 shell would develop when the cluster grows according to the mechanism proposed in Ref. [22]. We analyse a cluster of 8500 particles grown from a seed of 4500 particles at 1 bar and 245 K. We briefly explain first the way we look

p/bar	T/K	ΔT/K	N_c	$\Delta\mu$/(kcal/mol)	f^+/s^{-1}	$\rho_f/(g/cm^3)$	$\rho_s/(g/cm^3)$	$\gamma/(mJ/m^2)$	$\Delta G_c/(k_BT)$	$\log_{10}(Jm^3s)$
1	226.5	18.5	6583	0.074	1.7×10^{14}	1.00	0.954	29.9	542	-196

TABLE II. Variables involved in the calculation of the ice 0 nucleation rate and the water-ice 0 interfacial free energy of mW water. See main text for the meaning of all variables.

for ice 0 particles in such cluster. In Fig. 9(a) we show a $\bar{q}_4-\bar{q}_6$ map for 5000 bulk particles of the liquid, ice Ih, ice 0 and ice Ic phases at 245 K. The cut-off to find neighbour particles for the calculation of both $\bar{q}_4$ and $\bar{q}_6$ was set to 5 Å. In Fig. 9(b) we show with brown dots the $\bar{q}_4-\bar{q}_6$ map for all particles of the configuration of the grown cluster surrounded by the fluid. Distinct clouds for the fluid and ice Ih phases can be seen, as well as a 'bridge' joining both clouds. The bridge corresponds to interfacial particles having an order parameter in between that of the bulk phases. Only a couple of these particles falls in the order parameter region characteristic of bulk ice 0, indicated with a dashed ellipse in Fig. 9(b). In fact, the largest cluster of non-liquid particles in Fig. 9(c) shows only one ice 0 particle on its surface (in red). However, one could spuriously identify a shell of particles as ice 0 if, for the employed order parameter, the bridge of interfacial particles overlaps with the bulk ice 0 cloud. We illustrate this case in Figs. 9(d), (e) and (f), which correspond to a $\bar{q}_4-\bar{q}_6$ order parameter with a cut-off distance of 4.6 Å instead of 5 Å. Both order parameters (5 and 4.6 Å) are equally valid to distinguish liquid from either ice Ih or ice 0 because the clouds of the different bulk phases do not overlap with each other (Fig. 9(d)). However, the order parameter of interfacial particles bridging the liquid and the ice Ih cluster clouds now overlaps with the ice 0 cloud (Fig. 9(d)). As a consequence, the largest cluster of non-liquid particles is surrounded by particles spuriously identified as ice 0 (in red) that in reality are interfacial particles with an order parameter intermediate between that of the ice Ih and the liquid clouds. We believe that the $W_4, \bar{q}_4$ order parameter employed in Ref. [22] may have the same shortcoming as the $\bar{q}_4-\bar{q}_6$ used here with 4.6 Å cut-off. In fact, the ice 0 cloud shown in Fig. 6 of the Supplementary Material of Ref. [22] falls in between the liquid and the ice Ic clouds (the core of the clusters identified in Ref. [22] is mainly ice Ic).

In summary, this Supplementary Material on the one side confirms with the mW model the findings discussed in the main paper and on the other side dismisses the alternative explanation to the pressure effects on water freezing reported in Ref. [22]. Moreover, the results for the mW are a proof of concept for the seeding approach followed in our work: On the one hand, the nucleation rate predicted with seeding for high supercooling is consistent with brute force simulations. On the other hand, the extrapolation of the interfacial free energy obtained with seeding to 0 supercooling is consistent with direct calculations using the Mold Integration method.

We show that the mW qualitatively predicts the experimental observation that pressure slows ice nucleation. The quantitative agreement between mW and the experiment is not as good as that of the TIP4P/Ice model, though. As in the case of the TIP4P/Ice model, the slowing down of ice nucleation with pressure is due to a combined effect of the melting temperature, the chemical potential difference, the solid density and the ice I-water interfacial free energy, being the latter the predominant factor.

The interfacial free energy with the liquid is higher for ice 0 than for ice I. Therefore, ice 0 can not explain ice nucleation in mW. We argue that in Ref. [22] ice 0 was possibly mistaken with interfacial water.

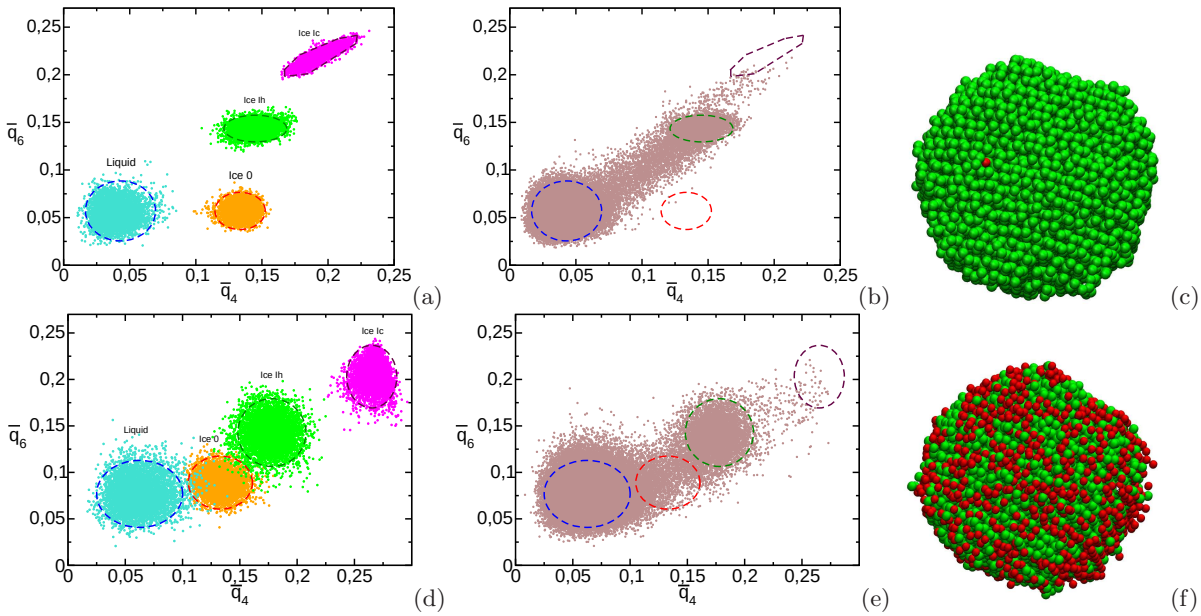

FIG. 9. (a) $\bar{q}_4, \bar{q}_6$ map for 5000 bulk mW liquid, ice Ih, ice Ic and ice 0 particles at 245 K and 1 bar using a 5 Å cut-off distance to compute the order parameter. (b) $\bar{q}_4, \bar{q}_6$ map for a configuration at 245 K and 1 bar containing a growing ice Ih cluster. For visual aid dashed ellipses have been drawn limiting the area within which most particles of the corresponding bulk phase are enclosed. (c) largest cluster of non-liquid particles ($\bar{q}_4 > 0.095$) in the configuration of the growing ice Ih cluster. In red, particles whose order parameter is enclosed within the ellipse surrounding the ice 0 cloud. (d), (e) and (f): same as (a), (b) and (c) but with a cut-off of 4.6 Å and a threshold of $\bar{q}_4 > 0.108$ to label non-liquid particles.

[1] S. Plimpton *J. Comput. Phys.*, vol. 117, p. 1, 1995.

[2] E. Lindahl, B. Hess, and D. van der Spoel, "Gromacs 3.0: a package for molecular simulation and trajectory analysis," *J. Mol. Model.*, vol. 7, p. 306, 2001.

[3] V. Molinero, and E. B. Moore, "Water modeled as an intermediate element between carbon and silicon," *The Journal of Physical Chemistry B*, vol. 113, no. 13, pp. 4008–4016, 2009.

[4] J. L. F. Abascal, E. Sanz, R. G. Fernandez, and C. Vega, "A potential model for the study of ices and amorphous water: TIP4P/Ice," *J. Chem. Phys.*, vol. 122, p. 234511, 2005.

[5] M. Parrinello and A. Rahman, "Polymorphic transitions in single crystals: A new Molecular Dynamics method," *J. App. Phys.*, vol. 52, pp. 7182–7190, 1981.

[6] G. Bussi, D. Donadio, and M. Parrinello, "Canonical sampling through velocity rescaling," *The Journal of Chemical Physics*, vol. 126, no. 1, p. 014101, 2007.

[7] D. R. Wheeler and J. Newman, "A less expensive ewald lattice sum," *Chem. Phys. Lett.*, vol. 366, p. 537, 2002.

[8] W. G. Hoover, "Canonical dynamics: Equilibrium phase-space distributions," vol. 31, p. 1695, 1985.

[9] W. G. Hoover, "Constant-pressure equations of motion," *Phys. Rev. A*, vol. 34, pp. 2499–2500, Sep 1986.

[10] S. Melchionna, G. Ciccotti, and B. L. Holian, "Hoover npt dynamics for systems varying in shape and size," *Molecular Physics*, vol. 78, no. 3, pp. 533–544, 1993.

[11] W. Lechner and C. Dellago, "Accurate determination of crystal structures based on averaged local bond order parameters," *J. Chem. Phys.*, vol. 129, no. 11, p. 114707, 2008.

[12] E. Sanz, C. Vega, J. R. Espinosa, R. Caballero-Bernal, J. L. F. Abascal, and C. Valeriani, "Homogeneous ice nucleation at moderate supercooling from molecular simulation," *Journal of the American Chemical Society*, vol. 135, no. 40, pp. 15008–15017, 2013.

[13] J. R. Espinosa, E. Sanz, C. Valeriani, and C. Vega, "Homogeneous ice nucleation evaluated for several water models," *J. Chem. Phys.*, vol. 141, p. 18C529, 2014.

[14] A. Zaragoza, M. M. Conde, J. R. Espinosa, C. Valeriani, C. Vega, and E. Sanz, "Competition between ices ih and ic in homogeneous water freezing," *The Journal of Chemical Physics*, vol. 143, no. 13, p. 134504, 2015.

[15] J. R. Espinosa, C. Vega, C. Valeriani, and E. Sanz, "Seeding approach to crystal nucleation," *J. Chem. Phys.*, vol. 144, p. 034501, 2016.

[16] J. R. Espinosa, C. Vega, and E. Sanz, "The mold integration method for the calculation of the crystal-fluid interfacial free energy from simulations," *J Chem. Phys.*, vol. 141, no. 13, p. 134709, 2014.

[17] J. R. Espinosa, C. Vega, and E. Sanz, "Ice-water interfacial free energy for the tip4p, tip4p/2005 , tip4p/ice and mw models as obtained from the mold integration technique," *The Journal of Physical Chemistry C*, vol. 120, pp. 8068–8075, 2016.

[18] A. Haji-Akbari and P. G. Debenedetti, "Direct calculation of ice homogeneous nucleation rate for a molecular model of water," *Proceedings of the National Academy of Sciences*, vol. 112, no. 34, pp. 10582–10588, 2015.

[19] E. B. Moore and V. Molinero, "Structural transformation in supercooled water controls the crystallization rate of ice," *Nature*, vol. 479, no. 7374, pp. 506–508, 2011.

[20] J. R. Espinosa, C. Vega, C. Valeriani, and E. Sanz, "The crystal-fluid interfacial free energy and nucleation rate of NaCl from different simulation methods," *J. Chem. Phys.*, vol. 142, no. 19, p. 194709, 2015.

[21] H. Kanno, R. J. Speedy, and C. A. Angell, "Supercooling of water to -92^{o}c under pressure," *Science*, vol. 189, no. 4206, pp. 880–881, 1975.

[22] J. Russo, F. Romano, and H. Tanaka, "New metastable form of ice and its role in the homogeneous crystallization of water," *Nature Materials*, vol. 13, p. 733, 2014.